

# **The influence of the ambient flow on the spreading of convected water masses**

by Sonya Legg<sup>1,2</sup> and John Marshall<sup>3</sup>

## **ABSTRACT**

We investigate the influence of a cyclonic vortical flow on the lateral spreading of newly mixed fluid generated through localized deep convection. Localized open ocean deep convection often occurs within such a cyclonic gyre circulation, since the associated upwardly domed isopycnals and weaker stratification locally precondition the ocean for deeper convection. In the absence of ambient flow, localized convection has been shown to result in strong lateral fluxes of buoyancy generated by baroclinic instability, sufficient to offset the local surface buoyancy loss and limit the density anomaly of the convectively generated water mass.

Here we examine the consequences of a cyclonic ambient flow on this baroclinic instability and lateral mixing. To isolate the influence of the circulation on this later stage of localized convection, we parameterize the convective mixing by the introduction of baroclinic point vortices (“hetons”) in a two-layer quasi-geostrophic model, and prescribe the initial flow by a patch of constant potential vorticity. Linear stability analysis of the combined system of pre-existing cyclonic vortex and convectively generated baroclinic vortex indicates scenarios in which the pre-existing cyclonic circulation can modify the baroclinic instability. Numerical experiments with the two-layer QG model show that the effectiveness of the lateral heat fluxes can be strongly diminished by the action of the pre-existing circulation, thereby increasing the density anomaly of the convected water mass.

## **1. Introduction**

In several recent studies of localized open ocean deep convection (Legg and Marshall, 1993; Send and Marshall, 1995; Visbeck *et al.*, 1996; Ivey *et al.*, 1995; Coates *et al.*, 1995; Brickman, 1995; Legg *et al.*, 1996) it has become clear that baroclinic instability of the localized convection site leads to significant lateral fluxes of buoyancy as fluid is transported away from and into the convecting site by finite amplitude eddies. These lateral fluxes may be large enough to completely offset the surface forcing. A statistically steady state may result, in which the density anomaly of the overturned fluid ceases to increase, and the deepening of the mixed layer is halted. If the lateral fluxes achieved by baroclinic instability were in any way rendered less effective, different water-mass properties would result.

1. Institute for Geophysics and Planetary Physics, University of California, Los Angeles, California, 90024; U.S.A.

2. Present address: Woods Hole Oceanographic Institution, Woods Hole, Massachusetts, 02543, U.S.A.

3. Department of Earth, Atmospheric and Planetary Sciences, MIT, Cambridge, Massachusetts, 02139, U.S.A.

Previous studies of localized convection have considered a convecting region within a volume of either infinite extent (Legg and Marshall, 1993; Legg *et al.*, 1996) or confined by the numerical domain (Jones and Marshall, 1993) or laboratory apparatus (Coates *et al.*, 1995; Brickman, 1995). Most of these studies assume a quiescent initial flow (although Ivey *et al.* (1995) considered a preconditioning flow driven by a rotating disc). Observations, however, reveal that convection often occurs within a local gyre circulation (Killworth, 1983). This may be associated with (i) local topographic features such as the Rhone fan in the northwest Mediterranean (Swallow and Caston, 1973; Hogg, 1973) or Maud Rise in the Weddell Sea (Gordon, 1978; Alverson and Owens, 1996), (ii) winter-time intensification of the wind-driven circulation (Pinardi and Navarra, 1993) or (iii) localized cooling such as that generated by winds blowing off the ice-sheet in the Labrador Sea (Clarke and Gascard, 1983; Seung, 1987) or a combination of all three processes. A cyclonic shear is associated with doming of isopycnals up to the surface and provides one of the “preconditioning” factors necessary for deep convection events. Since the eddies generated by baroclinic instability carry fluid out of the convecting region and into the ambient circulation, the spreading phase of deep-water formation should not be considered in isolation from the background flow. Recent observations in the Labrador Sea (Peter Rhines, personal communication, 1997) show significant barotropic eddy activity occurring at the time of deep convection, further motivating an investigation of the influence of barotropic flow on the convection and spreading.

Several recent studies have begun to examine the preconditioning of the ocean for locally deeper convection by the ambient circulation, including the flow trapped over topography (Alverson and Owens, 1996; Madec *et al.*, 1996), isolated geostrophic eddies (Legg *et al.*, 1998), and wind-driven barotropic gyres (Madec *et al.*, 1996). All of these studies show that in addition to influencing the localization of convection, the ambient flow may also influence the spreading of the convected fluid. Alverson and Owens (1996) show that baroclinic instability may be replaced by mean flow advection in the presence of a uniform flow, while Madec *et al.* (1996) suggest that a barotropic gyre circulation may suppress baroclinic instability of the convecting area. In this study we examine in detail the influences of ambient gyre flows associated with the preconditioning and wind-driven circulation on the development of baroclinic instability. We investigate in particular the possibility that this pre-existing circulation can affect the rate at which convected water subsequently spreads away from the formation region, and the efficiency with which baroclinic instability draws buoyancy into the convecting patch.

The influence of barotropic flow on baroclinic instability has been examined in the context of atmospheric baroclinic life cycles, where a “barotropic governor” (James, 1987) can suppress the eddy activity. In contrast to these zonal atmospheric flows, in the oceanic convection context both baroclinic and barotropic flows are localized within eddies or gyres, where the spatial scale of the localization can influence the stability.

We use a highly idealized model to capture baroclinic instability and its modification by the ambient circulation: a point vortex ‘heton’ model of the convecting process, embedded

within a contour-dynamical representation of the pre-existing circulation. The point-vortex model was introduced by Legg and Marshall (1993) (hereafter LM), and its efficiency and applicability in the study of the properties of the spreading phase of convection demonstrated by Legg *et al.* (1996) (hereafter LJV). The advantages of this Lagrangian formulation include its low cost, and the absence of boundaries or viscous processes. We regard the results of heton model experiments as providing a useful guide ranging across parameter space which can be investigated further by other (more expensive) numerical models containing more complete physics.

Through the combination of linear stability analyses (a variant on the results of Flierl (1988) and Nakamura (1993)) and numerical experiments using the heton model, we find that the addition of an ambient circulation comprising a vortex with a strong barotropic component can suppress the baroclinic instability of the convected region. The suppression of the instability is a consequence of the change in the absolute vorticity of the convective region, and along with it, stronger angular momentum constraints on the instability process. Associated with the reduction in instability, the lateral spreading of the overturned fluid is diminished, as are the lateral fluxes of buoyancy drawn into the convecting region from the periphery. We conclude that the properties of the mixed water will be altered by the presence of a barotropic swirl, with a smaller volume of denser water being generated.

In Section 2 we briefly review the properties of the heton model of the spreading phase of ocean convection from LM and LJV, and outline the potential vorticity representation of the preconditioned flow. After a discussion of the predictions for stability of the convected region deduced from linear theory in Section 3, numerical experiments using the Lagrangian quasi-geostrophic two-layer point vortex/contour dynamics model are described in Section 4, and the implications for deep-water formation discussed in Section 5.

## **2. A point vortex model of the convection region**

The localized convective mixing due to buoyancy forcing at the ocean surface leads to the generation of a density anomaly in the convected region, which under the influence of rotation and gravity relaxes to a state of geostrophic adjustment, with a baroclinic rim current associated with the region of dense fluid. The baroclinic structure of this geostrophically adjusted state can be represented most simply in a two-layer quasi-geostrophic model with a cyclonic flow in the upper layer and an anticyclonic flow in the lower layer. The ongoing forcing serves to transform the density of the fluid from that of the upper layer to that of the lower layer, thereby raising the interface between the layers in the forcing region. Prognostic equations in the quasi-geostrophic representation are given in terms of potential vorticity, which contain information on the velocity fields in addition to the density anomaly. We make a further discretization by representing the potential vorticity field in terms of an ensemble of point vortices. Since the potential vorticity anomaly associated with a density anomaly is baroclinic (the surface density anomaly is replaced by a potential vorticity anomaly placed beneath an isothermal surface as described by Bretherton (1966) and elucidated further in LM), the point vortex representation involves

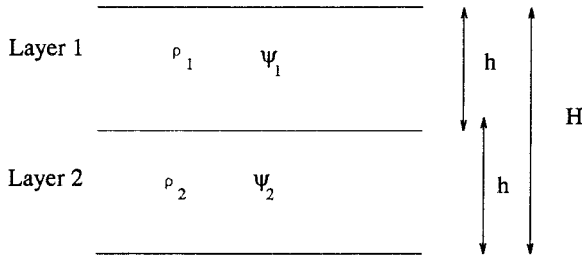


Figure 1. A schematic diagram showing the vertical structure of the two-layer quasi-geostrophic model. The layer depths,  $h$ , are equal, and the deformation radius  $\lambda = (g\Delta\rho h/(2\rho_0))^{1/2}/f$ , where  $\Delta\rho = \rho_2 - \rho_1$ .

baroclinic pairs of vortices, with cyclonic vortices in the upper layer and anticyclonic vortices in the lower layer. The term ‘heton’ has been coined to describe such a point vortex pair (Hogg and Stommel, 1985). This discretization results in a model of the development of the density anomaly and attendant geostrophic dynamics of considerable simplicity and economy, of which further details are given in Legg and Marshall (1993).

*a. The heton model: summary of previous results*

In the heton model a two-layer quasi-geostrophic model is used to represent the geostrophically adjusted convectively-mixed water column. The model is formulated in terms of potential vorticity with a baroclinic potential vorticity anomaly  $q^{bc}$  being related to a buoyancy anomaly  $b$  through

$$q^{bc} = -\frac{f}{N^2 H} b; q_1 = q^{bc}, q_2 = -q^{bc} \tag{1}$$

where

$$b = -g \frac{\Delta\rho}{\rho_0} \tag{2}$$

where  $g$  is the gravitational acceleration,  $f$  is the Coriolis parameter,  $\rho_0$  is the reference density,  $\Delta\rho$  is the density anomaly,  $N$  is the Brunt-Väisälä frequency, and  $H$  is the layer depth.  $q_1$  and  $q_2$  are the potential vorticity anomalies in the upper and lower layers respectively, with units of  $s^{-1}$ .  $N^2 = g/\rho_0(\rho_2 - \rho_1)/H$  where  $\rho_1$  and  $\rho_2$  are the densities of the upper and lower layer respectively (See Fig. 1). A surface buoyancy forcing  $B_0$  generates a buoyancy anomaly at a rate

$$\frac{db}{dt} = -\frac{B_0}{H} \tag{3}$$

so that

$$\frac{dq^{bc}}{dt} = R_q f^2 \quad (4)$$

where  $R_q = B_0/(H^2 N^2 f)$  is a nondimensional measure of the forcing strength.  $R_q$  represents the potential vorticity anomaly generated in time  $1/f$  as compared to the planetary vorticity  $f$ . As such  $R_q$  is similar to a Rossby number (relative vorticity compared to planetary vorticity). Oceanic values are typically very small ranging from  $10^{-5}$  for weak forcing and strong  $N$ , to  $10^{-1}$  for very strong forcing.

This potential vorticity anomaly is discretized into point vortices, to enable efficient computation, and provide a controllable element of randomness and clumping in the buoyancy forcing, mimicking the spatial fluctuations of the oceanic forcing. The number of point vortex pairs (hetons),  $\mathcal{N}$ , within the forcing disc of area  $A$  is related to  $q^{bc}$  by  $\mathcal{N} = q^{bc} A/s$  where  $s$  is the strength of the individual point vortices. Hence the rate of increase of hetons is given by

$$\frac{d\mathcal{N}}{dt} = \frac{AfB_0}{sN^2H^2} = \pi \left| \frac{r}{\lambda} \right|^2 \frac{R_q f}{S_p} \quad (5)$$

where  $\lambda = NH/(\sqrt{2}f)$  is a modified deformation radius;  $S_p = s/(\lambda^2 f)$  is a nondimensional vortex strength; and  $r$  is the radius of the circular disc over which cooling is applied. Physical results of the problem do not depend on  $S_p$  provided it is sufficiently small to allow the vortices to act as an ensemble.

In the numerical experiments of LM and LJV the dynamics of the convecting region in the absence of any ambient flow were investigated. In the reference experiment of LM a cooling is applied over the circular disc of a radius several times the deformation radius, generating a baroclinic potential vorticity anomaly at a rate given by (4), discretized by the addition of hetons (Fig. 2a). A sheared rim current is generated around the cooling region (Fig. 2b), which eventually becomes baroclinically unstable, allowing tilted clusters of hetons to break out of the cooling region (Fig. 2c). There is symmetry between the development of the instability in the upper and lower layers, so that the tilted heton clusters have approximately equal numbers of hetons in upper and lower layers, and can therefore self-propagate away from the convected region indefinitely (Fig. 2d). A statistically steady state is established after only a few days, in which the rate of generation of hetons is balanced by the rate at which they are fluxed out of the patch by baroclinic instability (Fig. 3). The implied lateral heat flux achieved by the migrating hetons is sufficient to completely balance the surface cooling. Since the number of hetons within the cooling region remains roughly constant at later times, the density anomaly of the overturned fluid does not increase further. LJV found simple scaling relationships for the equilibrium number of hetons in the patch and corresponding equilibrium buoyancy anomaly, as well as the time at which the breakup of the patch occurred. These relationships closely match their

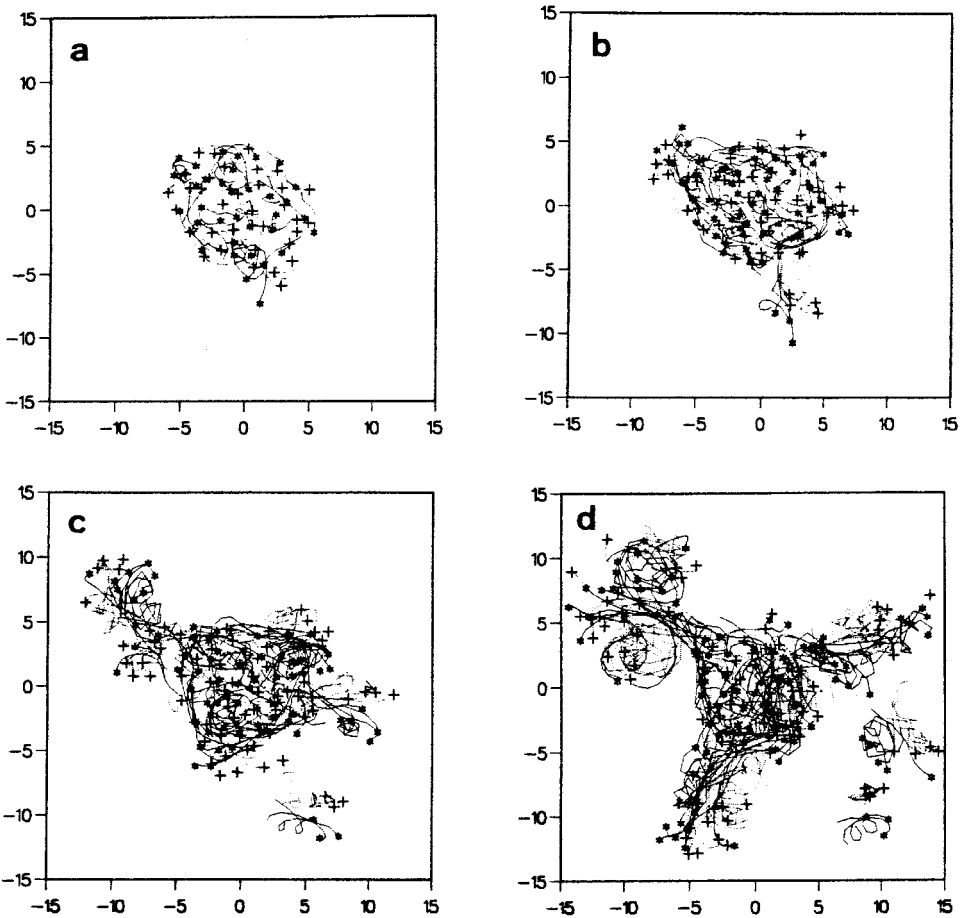


Figure 2. Four pictures charting the development of an evolving cluster of hetons in the reference experiment. Each picture shows the trajectories of the hetons over a period of  $6 \times (1/f)$ . The trajectories of the upper-layer vortices are shown by dotted lines, while those of the lower-layer vortices are shown by solid lines. A cross marks the position of an upper layer vortex at the end of its trajectory, while a lower-layer vortex is marked by an asterisk. The horizontal scale is presented in units of  $\lambda$  and the hetons are introduced over a disc of diameter  $5\lambda$ . The pictures are for the following periods; (a) 6 to  $12 \times (1/f)$ , (b) 12 to  $18 \times (1/f)$ , (c) 18 to  $24 \times (1/f)$ , (d) 24 to  $30 \times (1/f)$ .

predictions made using a simple theory of the statistically steady state in which the flux of dense fluid through the boundary of the forcing region balances the generation of dense fluid by the surface buoyancy anomaly, and the root mean square flux velocity across this boundary is proportional to the rim current. (A corresponding set of relationships are found by Visbeck *et al.* (1996) for simulations and laboratory experiments of convection into a continuously stratified fluid.)

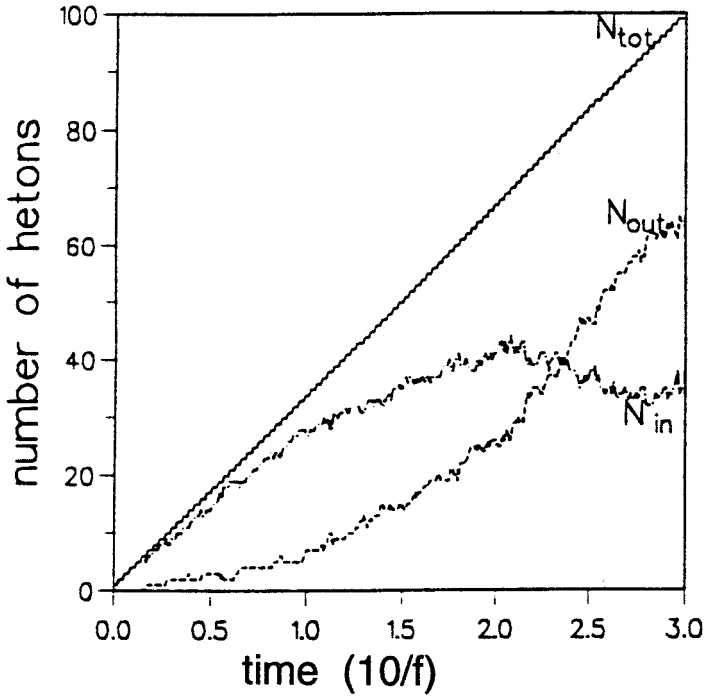


Figure 3. The evolution in time of the numbers of hetons:  $N_{tot}$ , the total number of hetons;  $N_{in}$ , the number of hetons within the forcing region;  $N_{out}$ , the number of hetons outside the forcing region; for the reference experiment.

Although each baroclinic point vortex pair is associated with a localized density anomaly, as an ensemble the hetons generate a density anomaly which decays over a finite distance, determined by the deformation radius, similar to that generated in a primitive equation model. (See LJV for comparison of density fields at similar stages of evolution for a primitive equation calculation and a heton model calculation of localized convection.)

LJV estimate the flux velocity from linear stability arguments (as in Stone, 1972), with the ratio between flux velocity and rim current velocity proportional to the growth rate of the instability (nondimensionalized by the potential vorticity anomaly). If these linear stability arguments to estimate flux velocity are applicable during the finite amplitude development of the instability, we would expect a decrease in growth rate to (a) increase the equilibrium density of the convected region (b) increase the time taken to reach equilibrium.

In the experiments to be described, the parameters will match those of LM, with a forcing parameter of  $R_q = 0.08$ , (corresponding to a surface cooling of  $\mathcal{H} = 800 \text{ W/m}^2$  into a two-layer fluid of depth 2 km and stratification  $N^2 = 5.0 \times 10^{-8} \text{ s}^{-2}$ ), a patch radius of  $r = 5\lambda$  (where  $\lambda = 1.58 \text{ km}$ ) and a nondimensional vortex strength of  $S_p = 1.9$ . It should be noted that the value of forcing given is stronger than usually found in convection

regions, while  $N^2$ ,  $r/\lambda$ , and  $\lambda$  are all smaller than typical values. The evidence of scaling behavior given in LJV allows us to have confidence that results will apply even for more typical values, and the present choice is a convenient computational one, allowing more rapid calculations. (A wide range of  $r/\lambda$  and  $R_q$  values are accessible—see LJV—but larger  $r/\lambda$  requires more individual vortices, while smaller  $R_q$  takes longer to reach equilibrium, both increasing the time of computation). The breakup time scale in this reference experiment is  $T_b = 15(1/f)$ , to which the development time scales in the presence of ambient flow will be compared. To represent the larger scale preconditioned flow, we use a patch of piece-wise constant potential vorticity to induce a large-scale swirl and employ a mixture of contour dynamics (see Appendix B) and point vortex techniques.

### *b. A potential vorticity representation of the ambient flow*

We focus on two different aspects of the pre-existing circulation in the convecting region. The first is the surface-intensified cyclonic circulation in geostrophic wind balance with the domed “preconditioned” density profile, of which numerous observations exist. Lazier (1973) and Clarke and Gascard (1983) in the Labrador Sea, recorded a surface density anomaly of  $\sigma'_T \sim 0.6 \text{ kg m}^{-3}$  over an area 200 km across, associated with a doming of isopycnals and supporting a cyclonic circulation. Similarly, Swallow and Caston (1973) observe surface density anomalies of magnitude  $\sigma'_T \sim 0.1 - 0.2 \text{ kg m}^{-3}$  in the Mediterranean, (Fig. 4), over an area 75 km across in the east-west direction, and 30 km across in the north-south direction. Associated with the density anomaly are cyclonic geostrophic shears of  $\sim 5 \text{ cm s}^{-1}$  over a radius of 20 km, confined mainly to the upper 200 m, in the Mediterranean, and  $\sim 15 \text{ cm s}^{-1}$  in the Labrador Sea. Inspection of the vertical profile of the density structure reveals that the density anomaly extends to about 500 m in the Mediterranean, and 1000–1500 m in the Labrador Sea. The vertical structure of the velocity profile is less clear, but a deep cyclonic shear of about 0.05 cm/s at 1500 m, relative to 2000 m is deduced in the Mediterranean (Swallow and Caston, 1973).

The second aspect of the pre-existing flow which we will consider is the barotropic component of the circulation, poorly estimated from observations, but available from numerical simulations forced by climatological surface wind stresses. Numerical simulations such as that of Zavatarelli and Mellor (1995) reveal a barotropic cyclonic gyre in the Gulf of Lions of maximum intensity during the winter, with velocities of a few  $\text{cm s}^{-1}$ . Modeling of the circulation associated with convection over Maud Rise (Alverson and Owens, 1996) indicates that a strong barotropic (anticyclonic) circulation can develop as a “Taylor cap” flow.

We represent these two aspects of the ambient flow—the surface density anomaly, and the barotropic vortical flow—using piece-wise constant potential vorticity distributions. The anomaly is chosen to be of a similar spatial dimension to the convective chimney, since it is likely that the preconditioned flow coincides with the area where overturning takes place. We will assume that the ambient circulation takes the form of a circular cyclonic vortex, of radius  $b$ , with the baroclinic convectively generated vortex of radius  $a$

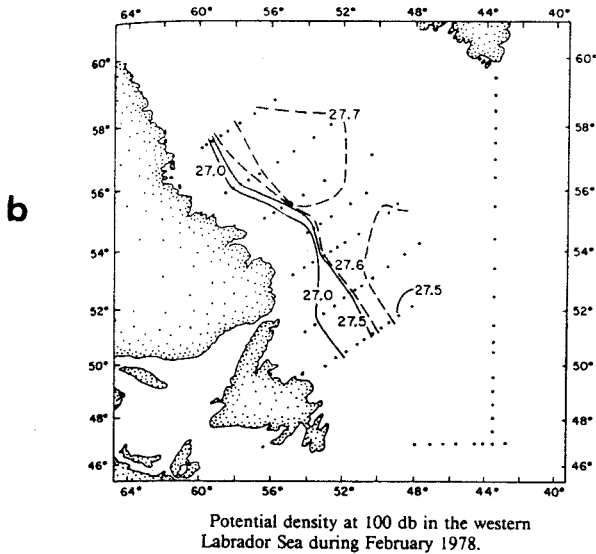
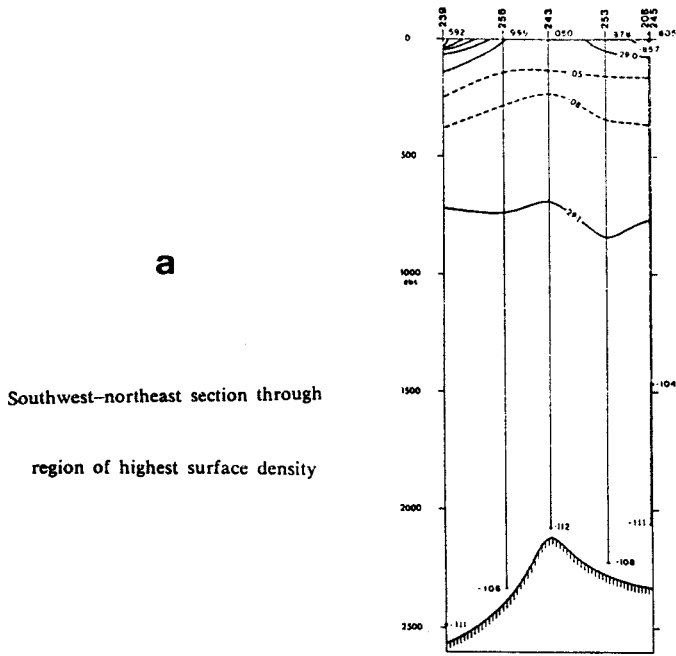


Figure 4. Observations of (a) the preconditioned potential density section through the region of highest surface density in the Gulf of Lions, Mediterranean Sea (from Swallow and Caston, 1973) and (b) the preconditioned potential density anomaly at 100 db in the Labrador Sea (from Gascard and Clarke, 1983), showing the existence of a region of weaker initial stratification associated with the doming of isopycnals to the surface.

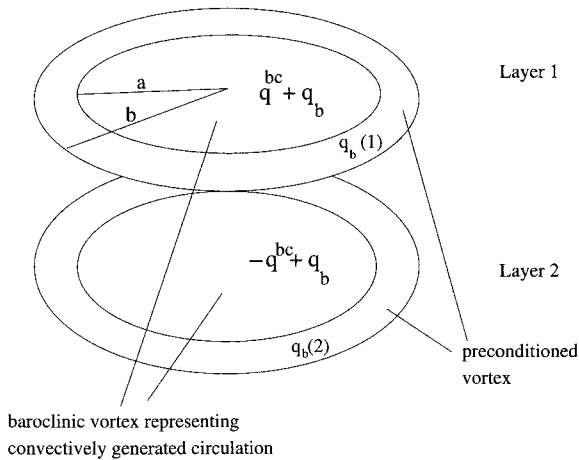


Figure 5. The potential vorticity structure of the baroclinic convectively generated vortex of radius  $a$  contained within a preconditioned flow of radius  $b$ , with potential vorticity anomaly  $q_b$ .

embedded within it (Fig. 5). The two different representations of the ambient flow that we will examine are (see Fig. 6): (case i) anomalously high potential vorticity extending through both layers, equivalent to a barotropic cyclonic flow with no density anomaly ( $q_1 = q_2 > 0$ ) (where we are considering the preconditioned vortex potential vorticity anomaly only), and (case ii) high potential vorticity confined to the upper layer only, ( $q_1 > 0$ ;  $q_2 = 0$ ), representing a positive surface density anomaly, invoking the ideas of Bretherton (1966). Case (ii) is associated with a cyclonic shear with height, corresponding to a reduction in the stratification in the center of the vortex, consistent with the preconditioning context. The ambient flow in the convecting region in nature probably contains a mixture of these two features. The results for an anticyclonic barotropic vortex would be completely analogous to those of the cyclonic barotropic vortex. Prior to the generation of a baroclinic potential vorticity anomaly by surface buoyancy forcing, both forms of preconditioned circulation are stable to baroclinic instability.

### 3. Predictions from linear stability analysis

Details of the linear stability analysis of a circular baroclinic vortex representing the circulation generated through convection, embedded in a barotropic vortex representing the preconditioned circulation, are given in Appendix A. Here only the salient points are outlined, followed by a finite amplitude investigation using contour dynamics.

We examine the stability of two piece-wise constant concentric vortices in each layer, of radius  $a$  (the baroclinic vortex of potential vorticity  $q^{bc}$ ) and radius  $b$  (the barotropic vortex of vorticity anomaly  $q^{bt}$  in case i, or the vortex of potential vorticity anomaly  $q^0$  in the upper layer, with no signal in the lower layer in case ii) (Fig. 5). This piece-wise constant representation forces the change in surface density anomaly to be very abrupt, and is

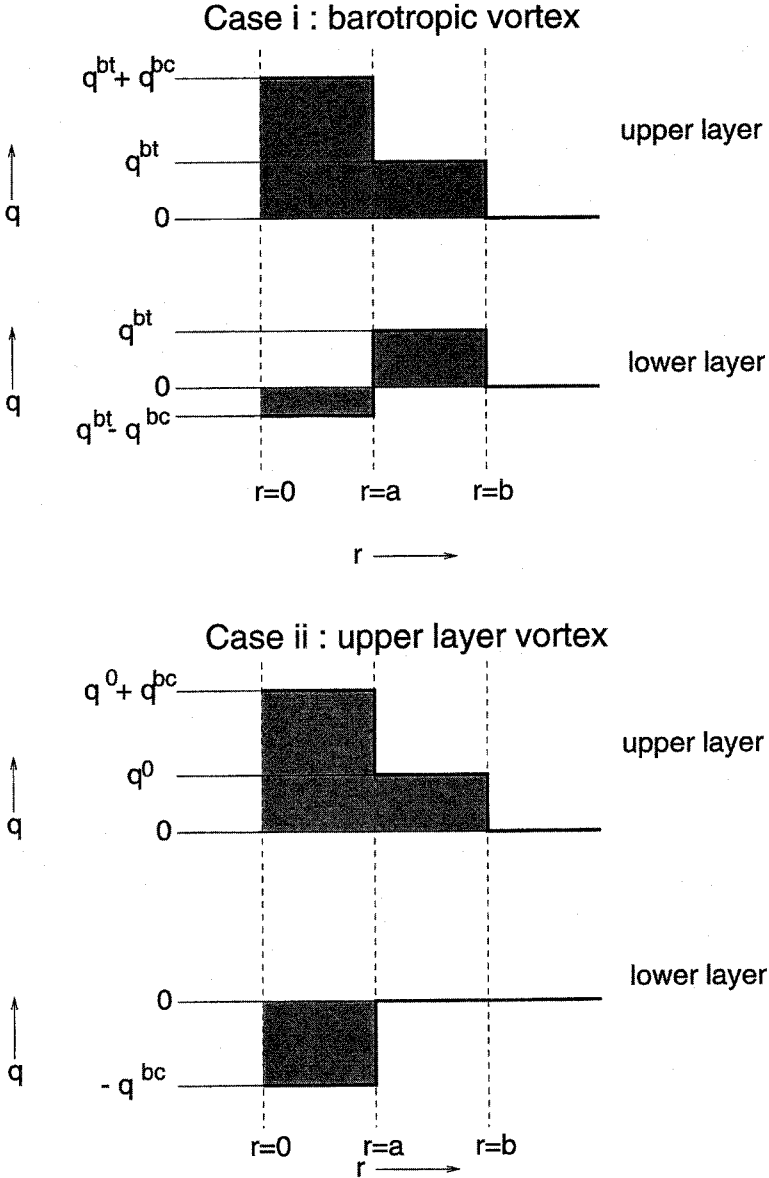


Figure 6. The total potential vorticity anomaly as a function of radius for two different preconditioned vortex scenarios. Case i: The preconditioned circulation is independent of  $z$ , so that in addition to the baroclinic component of the potential vorticity anomaly,  $q_{bc}$  of radius  $a$ , a barotropic component,  $q_{bt}$  of radius  $b$ , is added to both layers. Case ii: A preconditioned potential vorticity  $q_0$  of radius  $b$  is added to the upper layer only.

therefore rather more extreme than found in nature. However, an advantage of this representation is the relative simplicity of the linear stability analysis. In the atmospheric context Nakamura performed a linear stability analysis of a two-layer QG zonal flow separated into three distinct regions, analogous to our inner vortex, outer vortex and exterior region. However, he examined jet-like baroclinic and barotropic flow only for coincident baroclinic and barotropic jets. By contrast we examine cases where baroclinic and barotropic jets need not be coincident. Like Flierl (1988), we examine axisymmetric eddy flow in which the eddy size is an additional important parameter, rather than zonal flow as in Nakamura (1993).

The linear stability analysis indicates that in the case of a pre-existing circulation independent of height (case i), instability of the convected region can be completely suppressed if the baroclinic convectively generated potential vorticity anomaly is of a lesser magnitude than the pre-existing barotropic anomaly; as shown by Flierl (1988),  $|q^{bc}| > |q^{bt}|$  is a necessary condition for instability (see Fig. 6). (This also corresponds to the necessary condition for instability from the Charney-Stern theorem (Charney and Stern, (1962).) When the barotropic potential vorticity is of lower magnitude, instability occurs with a reduced growth rate (Fig. 17a).

Extension of Flierl's analysis to barotropic and baroclinic circulations of different radii (see Appendix A) shows that the suppression of the instability can only occur when the pre-existing vortex and convectively generated vortex are of similar size. If the boundaries of the two vortices are separated by more than a few deformation radii, they no longer influence one another.

In case ii—the preconditioned vortex with cyclonic vorticity in the upper layer only—instability is always possible, no matter how large the preconditioned potential vorticity anomaly. Furthermore, for the fastest growing mode, the growth rate is increased (Fig. 17b) when  $a = b$ .

Purely barotropic instability could occur if the potential vorticity jumps were of opposite sign at  $r = a$  and  $r = b$ , but of the same sign in each of the two layers. However, this does not fall within the regime we have selected, where the potential vorticity of vortex radius  $a$  is entirely baroclinic.

Motivated by the results of the linear stability analysis, we examine the finite-amplitude development of the baroclinic instability of a circular piece-wise constant vortex, in each scenario. A similar study was performed by Helfrich and Send (1988), and we extend their work to include concentric vortices of different sizes. As in the stability analysis, we examine the development of two piece-wise constant concentric vortices in each layer, with potential vorticities corresponding to case (i) or case (ii) as above. In case i, in agreement with the predictions of the linear stability analysis, we find that when  $b = a$ , instability is prevented for values  $q^{bt}/q^{bc} > 1$  (Fig. 7d). At lower values of  $q^{bt}/q^{bc}$ , the instability is suppressed particularly in the upper layer (which has potential vorticity of the same sign as the barotropic potential vorticity), while the perturbation grows in the lower layer (Fig. 7b,c). However, the mechanism for self-propulsion of potential vorticity

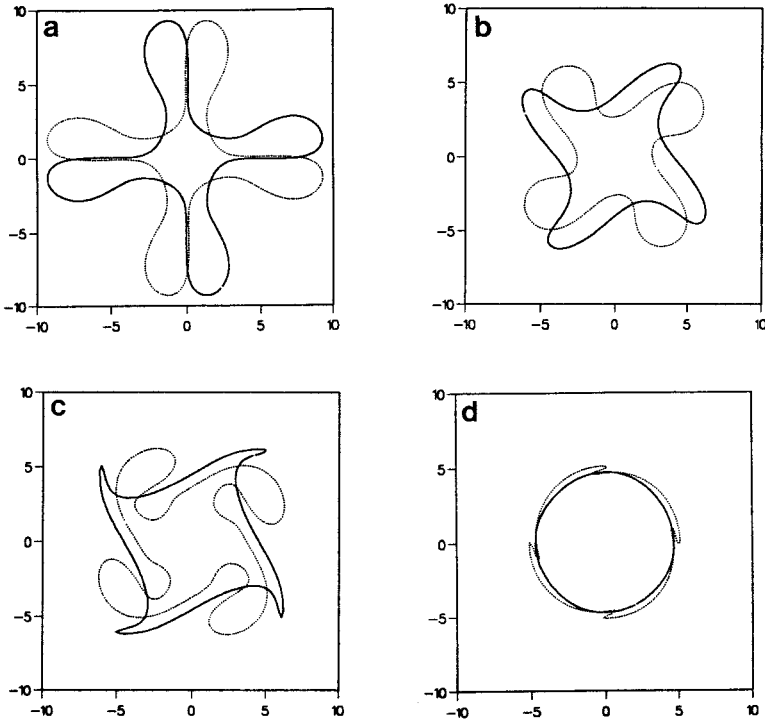


Figure 7. Results of numerical integrations using contour dynamics, showing the evolution of a baroclinic vortex of radius  $r = a$  contained within a vortex of radius  $r = b$ . Case i:  $q_b = q^{bt}$ , independent of  $z$ . In all cases vortex  $a$  is of radius  $a = 5\lambda$  and has potential vorticity anomaly  $q_a = q^{bc}$  in the upper layer, and  $q_a = -q^{bc}$  in the lower layer. The radii of the barotropic and baroclinic circulations are equal:  $a = b$ , and hence the vortex boundaries are coincident at all times, since they are material surfaces.  $q^{bt}$  takes values (a) 0, (b)  $0.2q^{bc}$ , (c)  $0.5q^{bc}$ , (d)  $1.0q^{bc}$ . The contour positions at a time of about  $8 \times (1/q^{bc})$  are shown for all cases, with the solid and dotted lines representing the upper and lower layer boundaries respectively. The tendency for the meanders to grow in the lower layer only as  $q^{bt}/q^{bc}$  increases is demonstrated, while when  $q_{bt}/q^{bc} = 1$ , the instability is completely suppressed.

anomalies outward is no longer present. Any clusters which break off from the main vortex contain predominantly lower-layer vorticity, so that they remain close to, and circle around the main vortex, in accord with the results of Helfrich and Send (1988). If  $b$  is much larger than  $a$ , we find that, as predicted, instability takes place even at large values of  $q^{bt}/q^{bc}$  (Fig. 8). However, as the tilted vortex dipoles move outward, they eventually come close enough to the boundary of the barotropic vortex to interact with it, and any further outward movement is prevented. For lower values of  $q^{bt}/q^{bc}$  the translating baroclinic dipoles cause fragments of the barotropic vortex to be ejected in their path.

In the finite amplitude integrations corresponding to case (ii), where the preconditioned vortex of radius  $b$  has potential vorticity anomaly  $q^0$  in the upper layer, and zero potential

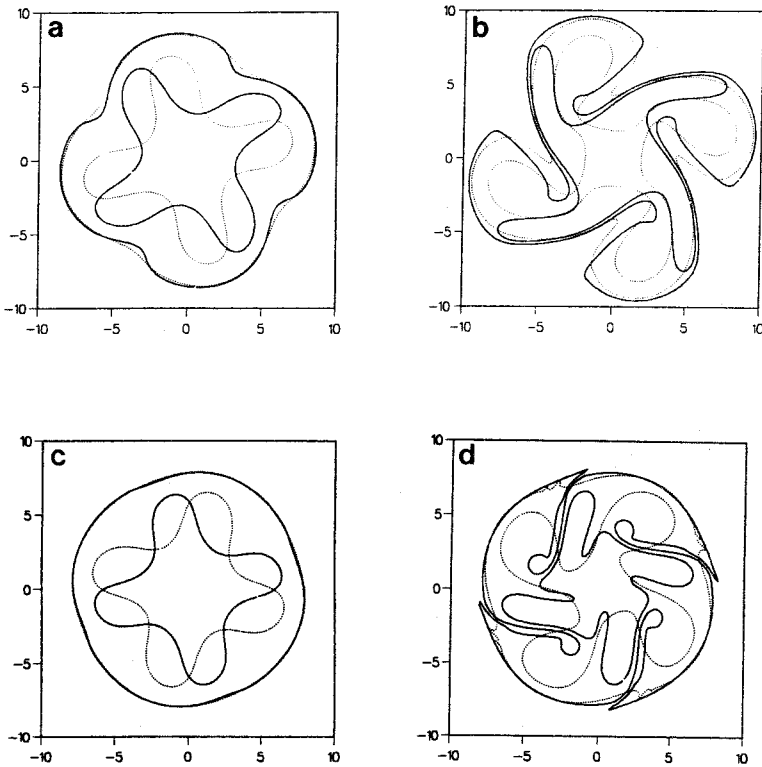


Figure 8. As for Figure 7, but with larger outer vortex radii  $b$ ;  $b = 8\lambda$ . (a)  $q^{bt} = 0.2q^{bc}$ ,  $t = 8 \times (1/q^{bc})$  (b)  $q^{bt} = 0.2q^{bc}$ ,  $t = 11 \times (1/q^{bc})$  (c)  $q^{bt} = 1.0q^{bc}$ ,  $t = 8 \times (1/q^{bc})$ , (d)  $q^{bt} = 1.0q^{bc}$ ,  $t = 14 \times (1/q^{bc})$ . Initially the development of the instability is unhindered, and the lobes of the baroclinic vortex are symmetrical between upper and lower layers, but at later times, greater development of the lower layer lobes, (b), or inability of the instability to develop further, (d), is evidence of the influence of the barotropic outer vortex.

vorticity anomaly in the lower layer, the baroclinic vortex of radius  $a$  and baroclinic potential vorticity  $q^{bc}$  is always unstable, as predicted by the linear stability theory. However, the meanders develop predominantly in the lower layer, which has potential vorticity of opposite sign to the barotropic component of the flow, resulting in a spreading of fluid in the lower layer only. During the instability of a purely baroclinic vortex (Fig. 7a) dipolar eddy structures are created possessing a symmetry between meander development in upper and lower layers; the self propagation of these dipoles fluxes fluid very efficiently out of the patch. However, when the meanders occur in the lower layer only, as in case (ii), this mechanism for propulsion of fluid out of the patch is removed (Fig. 9).

Similar calculations (not shown) with anticyclonic barotropic vorticity confirm that analogous behavior occurs, but with meanders occurring predominantly in the upper layer (where  $q^{bc}$  is of opposite sign to  $q^{bt}$ ).

Based on these results, one would expect baroclinic instability to be prevented from occurring in a convecting region embedded in a barotropic circulation at sufficiently high values of  $q^{bt}/q^{bc}$  when  $b = a$ . Lateral spreading of the lower layer anomaly would be greater than that of the upper layer for intermediate values of  $q^{bt}/q^{bc}$ , for cyclonic  $q^{bt}$ . (Spreading of the cyclonic upper layer would be greater for anticyclonic  $q^{bt}$ .) When the preconditioned vortex is significantly larger than the baroclinic convectively generated vortex, we do not expect the instability to be suppressed initially. When the meanders of the convective vortex boundary have propagated out to the boundary of the preconditioned vortex the instability may then be suppressed (Fig. 8). A pre-existing circulation consisting of cyclonic vorticity in the upper layer only, while it does not suppress the initial instability and may even enhance it, alters the finite amplitude development.

#### 4. Numerical experiments with hetons in a preconditioned flow

The numerical experiments to be described are based on the “reference” experiment of LM outlined earlier, with hetons of strength  $s = 1.9\lambda^2 f$  being added at a constant rate given by (5) randomly positioned over a disc  $10\lambda$  in diameter. (See Legg and Marshall (1993) for details.) However, now a barotropic circulation is added, represented by an initially circular patch of piece-wise constant potential vorticity. Three different possible pre-existing vortex scenarios are investigated, selected using results from our linear stability analysis as a guide. It should be recalled that a preconditioned vortex with a potential vorticity larger than the magnitude of the baroclinic potential vorticity anomaly of the convectively generated circulation is required, in order to suppress the baroclinic instability. Hence, since the maximum value of baroclinic potential vorticity anomaly in the reference experiment is  $q \approx 0.95f_0$ , we select a preconditioned vortex with  $q^{bt} = f_0$  (case i) or  $q^0 = f_0$  (case ii). (Later discussion will show that for more typical forcing strengths and length scales, smaller, more realistic values of  $q^{bt}$  will be sufficient.) In order to investigate the influence of the vortex size, we examine case (i) with a radius of  $b = 6\lambda$  and  $b = 8\lambda$ . (The radius of the baroclinic vortex is  $a = 5\lambda$ .) Hence our three different ambient circulation scenarios are as follows: a vortex of radius  $6\lambda$ , and potential vorticity anomaly of  $f_0$ , independent of  $z$ , (Fig. 10); a vortex of radius  $8\lambda$  and potential vorticity anomaly of  $f_0$ , independent of  $z$ , (Fig. 12); and a vortex of radius  $6\lambda$  with a potential vorticity anomaly of  $f_0$ , in the upper layer only, (Fig. 14).

##### *a. The evolution of the heton cluster in the presence of a barotropic vortex of radius $6\lambda$*

The first experiment (Fig. 10) lies in the regime where linear theory suggests baroclinic instability will be absent until the baroclinic potential vorticity anomaly is greater in magnitude than the barotropic, pre-existing anomaly. The results of the experiment show that, as expected, the ability of baroclinic instability to form self-propelling dipoles which flux the overturned fluid efficiently out of the cooling patch is severely reduced. The

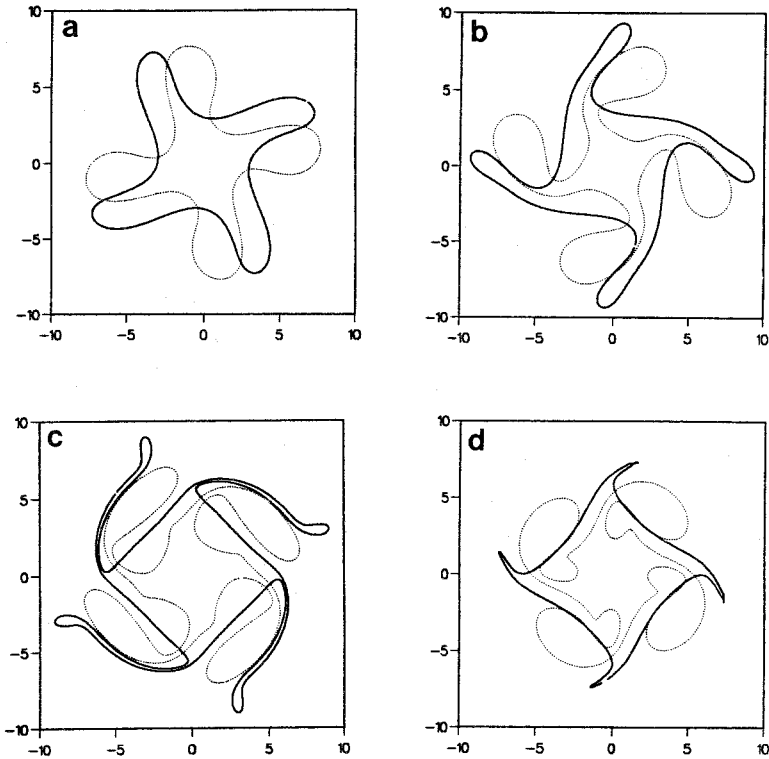


Figure 9. Results of numerical integrations using contour dynamics, showing the evolution of a baroclinic vortex of radius  $r = a$  contained within a vortex of radius  $r = b$ . Case ii:  $q_b = q_0$  in the upper layer and  $q_b = 0$  in the lower layer. In all cases the inner vortex has radius  $a = 5\lambda$  and potential vorticity anomaly  $q_a = q^{bc}$  in the upper layer, and  $q_a = -q^{bc}$  in the lower layer. The radii of the preconditioned and baroclinic circulations are equal:  $a = b$ , so that one boundary encloses both the baroclinic and additional potential vorticity anomalies.  $q_0$  takes values (a)  $0.2q^{bc}$ , (b)  $0.5q^{bc}$ , (c)  $1.0q^{bc}$  and (d)  $2.0q^{bc}$ . As in Figure 7, the dotted line represents the lower layer contour, with the solid line representing the upper layer, and positions are shown at about  $8 \times (1/q^{bc})$ . As  $q^0/q^{bc}$  increases, the meanders tend to grow only in the lower layer.

behavior of vortices is markedly different in the upper and lower layers, with lower-layer vortices being fluxed efficiently out of the patch, the numbers of lower-layer vortices within the patch remaining approximately steady after  $t = 15/f$ ; while the number of vortices in the upper layer continues to increase steadily (Fig. 11). The symmetry between the development of the instability in the upper and lower layers present in the reference experiment (Fig. 2d) has therefore been removed by the presence of the barotropic anomaly.

The time scale for the lower-layer vortices to reach a quasi-steady state is similar to the time scale for both layers in the reference experiment (Fig. 3), suggesting that in this layer, the efficiency of the flux velocity is unaltered.

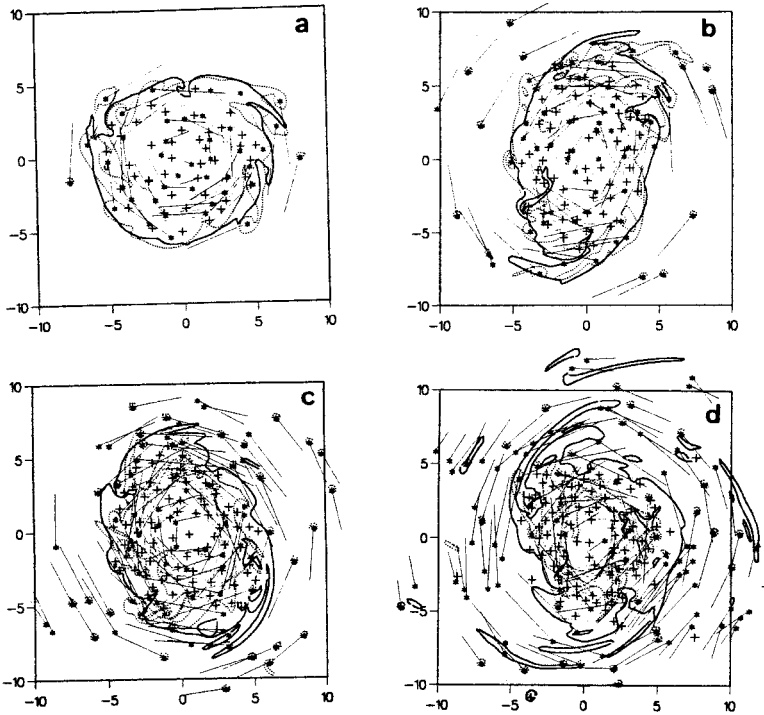


Figure 10. Four pictures charting the development of an evolving cluster of hetons contained within a barotropic vortex of radius  $6\lambda$  and potential vorticity  $q_{br} = f_0$ , independent of  $z$ . Each picture shows the trajectories of the hetons over a period of  $0.3 \times (1/f)$ , and the position of the boundary of the barotropic vortex at the end of that period. The trajectories of the upper layer vortices are shown by dotted lines, with a cross marking the end of the trajectory, while those of the lower layer vortices are shown by solid lines, with an asterisk marking their final position. The vortex boundary is shown by a solid line in the upper layer, and a dotted line in the lower layer. The horizontal scale is presented in units of  $\lambda$  and the hetons are introduced over a disc of diameter  $5\lambda$ , with a strength  $s = 0.6\pi\lambda^2f$ , at a rate corresponding to a cooling of  $800 \text{ Watts/m}^2$ , as in the reference experiment. The pictures are for the periods ending at the following times; (a)  $12 \times (1/f)$ , (b)  $18 \times (1/f)$ , (c)  $24 \times (1/f)$ , (d)  $30 \times (1/f)$ .

If the population of vortices and their rate of increase (Fig. 11) are interpreted in terms of the implied buoyancy fluxes, about half of the surface buoyancy loss is offset by the lateral fluxes affected by the lower-layer vortices, while the other half is serving to increase the density anomaly of the fluid in the overturning region. A statistically steady state exists in the lower layer, but not in the upper layer. Hence unlike the reference experiment, the density anomaly of the convecting region continues to increase indefinitely.

*b. The evolution of the heton cluster in the presence of a barotropic vortex of radius  $8\lambda$*

In the second experiment (Fig. 12), the heton cluster initially behaves much the same as in the reference experiment, although with a solid body rotation superimposed upon the

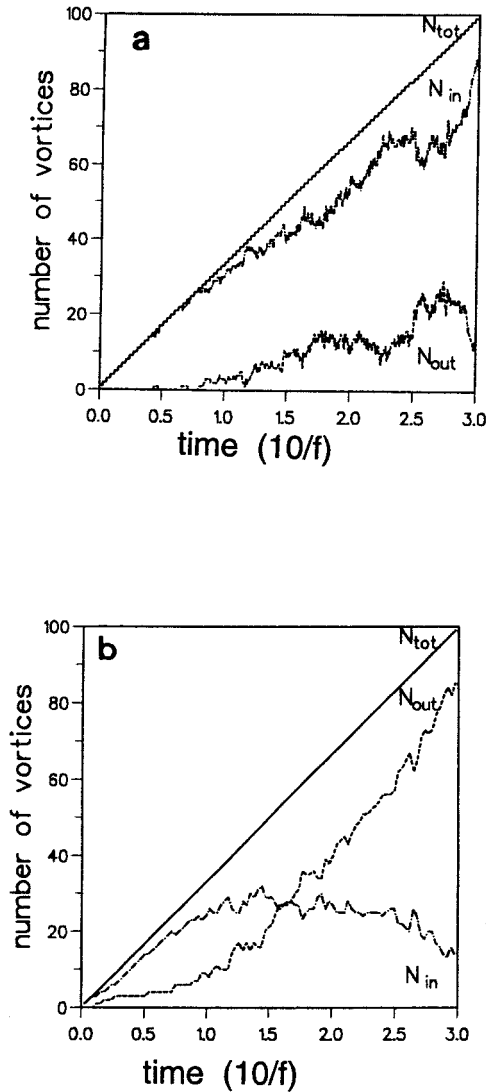


Figure 11. The evolution in time of  $\mathcal{N}_{tot}$ ,  $\mathcal{N}_{in}$ ,  $\mathcal{N}_{out}$  in (a) the upper layer, and (b) the lower layer, in the presence of a barotropic preconditioned circulation of strength  $f_0$  and radius  $6\lambda$ . The lower layer values were only sampled every 6 time-steps, resulting in a less noisy signal.

velocities. The number of vortices contained within and without the cooling region is initially symmetric between the two layers (Fig. 13), and identical to that of the reference experiment. Breakup of the cluster begins at about  $15 \times (1/f)$ , indicated by a rise in the number of vortices lying outside the cooling region, as in the reference experiment (Fig. 3). However, at about  $t = 18 \times (1/f)$ , (Fig. 12b), the tilted heton clumps have propagated

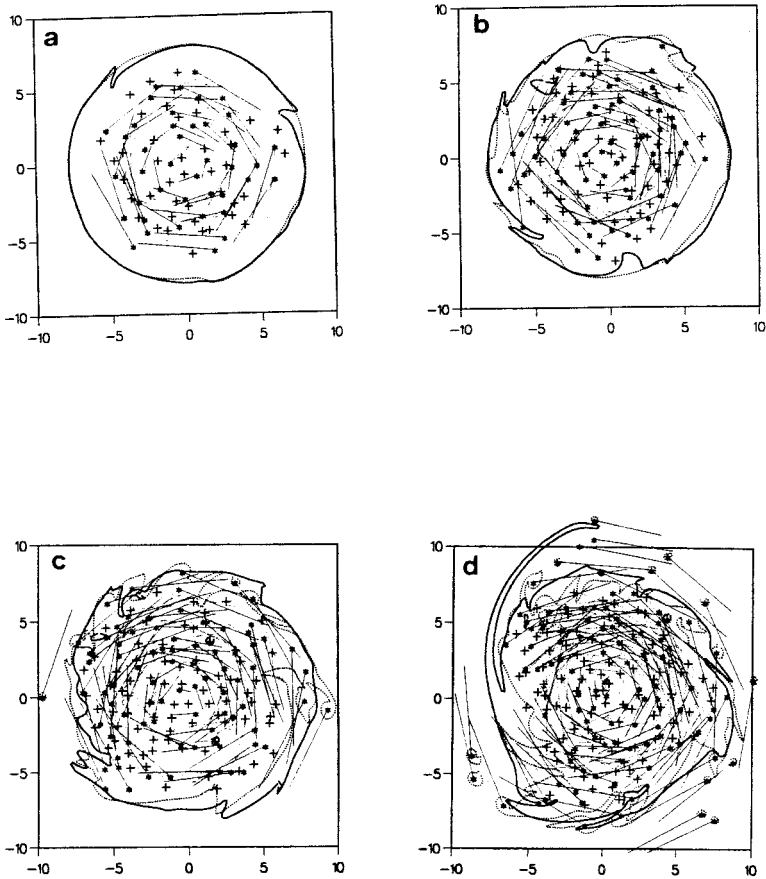


Figure 12. As for Figure 10, but where the barotropic vortex now has a radius of  $b = 8\lambda$ .

sufficiently close to the larger pre-existing vortex boundary to interact with it. As above, the lower-layer vortices continue to be fluxed out of the region, but the cyclonic vortex prevents the upper layer vortices from escaping. The number of lower-layer vortices within the forcing region reaches an equilibrium, while the number of upper layer vortices continues to rise.

At later stages several processes combine to balance the surface buoyancy loss: half of it is balanced by the lateral flux of buoyancy achieved by migration of the lower-layer vortices; one quarter is balanced by the lateral flux of buoyancy due to the upper-layer vortices migrating out of the cooling region, but unable to move further out than the boundary of the barotropic vortex at  $8\lambda$ ; one quarter serves to increase the density anomaly of the overturned region. Hence the density anomaly does not reach a statistically steady state.

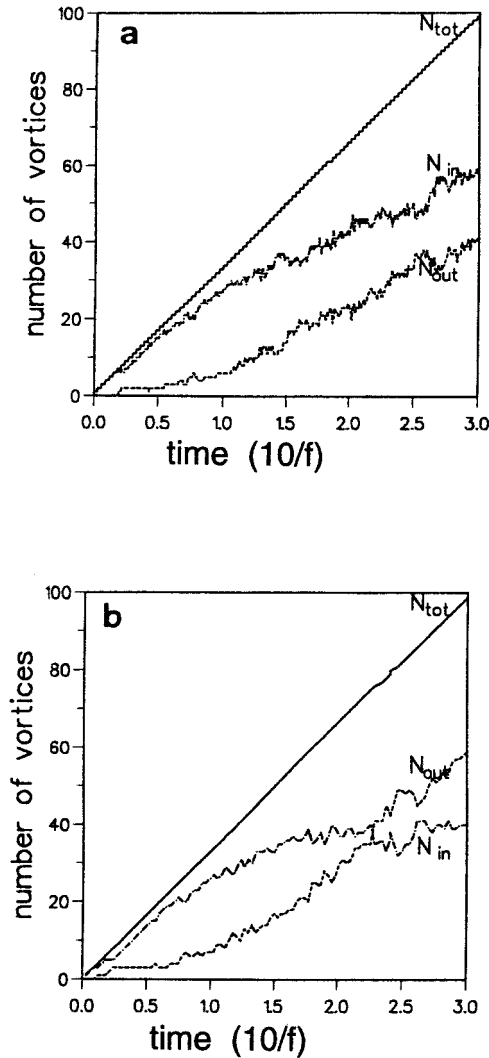


Figure 13. The evolution in time of  $\mathcal{N}_{tot}$ ,  $\mathcal{N}_{in}$ ,  $\mathcal{N}_{out}$  in (a) the upper layer, and (b) the lower layer, in the presence of a barotropic preconditioned circulation of strength  $f_0$  and radius  $8\lambda$ .

*c. The evolution of the heton cluster in the presence of a upper-layer preconditioned vortex of radius  $6\lambda$*

The third experiment contains a preconditioned vortex in the upper layer only. In this case, at about  $12 \times (1/f)$  (Fig. 15b), when the baroclinic circulation is of sufficient magnitude, clusters of lower-layer vortices move outward (Fig. 14). This breakup of the lower layer is more rapid than in the reference experiment (Fig. 3), suggesting a more efficient flux generated by the instability, in accordance with the higher growth rate

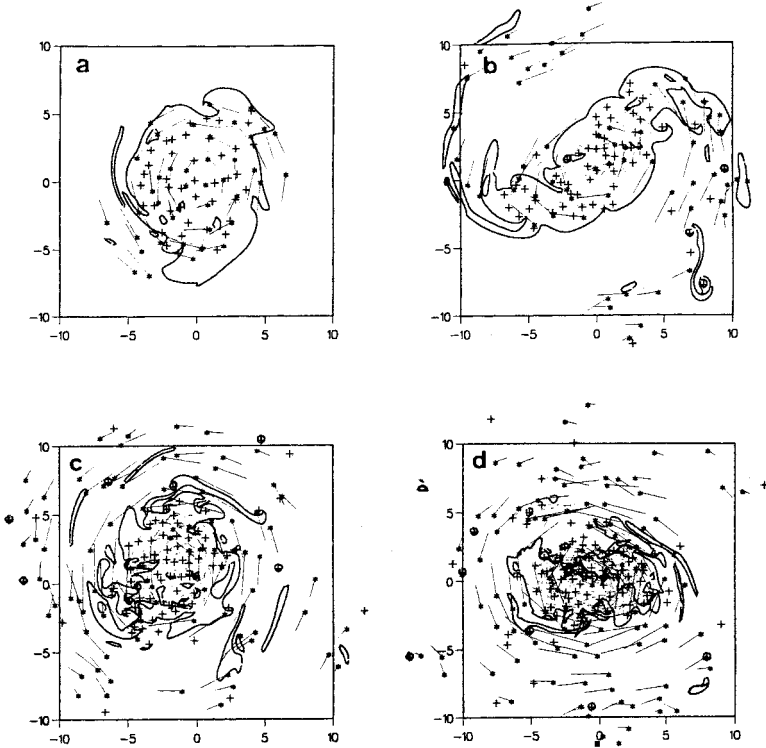


Figure 14. As for Figure 10, but where the heton cluster is contained within a vortex of radius  $6\lambda$  having a potential vorticity anomaly in the upper layer only, of strength  $q_0 = f_0$ , corresponding to case ii in the text.

indicated by linear theory. However, without a cyclonic partner, these clusters are unable to selfpropell very far and they circle the cooling region. On the long term, it appears that, as in the first heton/contour experiment, the lateral buoyancy flux is achieved solely by the lower-layer vortices, which have reached a statistically steady state. However, the density anomaly continues to rise due to the trapped upper-layer vortices.

*d. Discussion*

These heton experiments, (Figs. 10, 12, 14), exhibit much of the behavior of the experiments performed with contour dynamics alone, described in Section 3. For example, when the barotropic vortex is of approximately the same size as the cooling region, instability is suppressed until there are sufficient hetons to induce a baroclinic PV greater than the barotropic PV. When instability occurs, lower-layer hetons preferentially migrate outward, but remain close to the cooling region, so that the efficiency of the instability in transporting fluid far from the cooling region is suppressed. When the barotropic vortex is much larger than the baroclinic vortex, instability is not suppressed until migration of heton

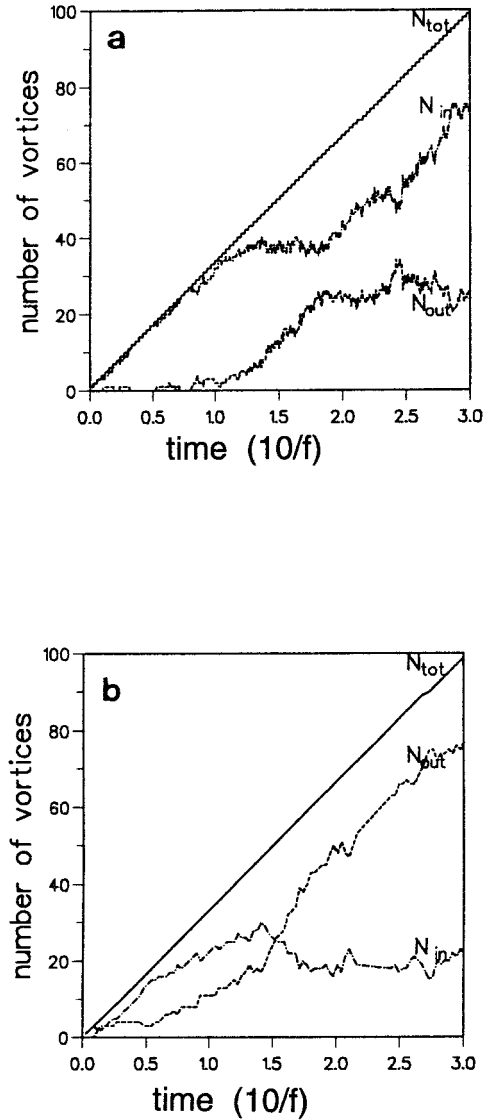


Figure 15. The evolution in time of  $\mathcal{N}_{tot}$ ,  $\mathcal{N}_{in}$ ,  $\mathcal{N}_{out}$  in (a) the upper layer and (b) the lower layer in the presence of a preconditioned circulation of strength  $f_0$  in the upper layer only, of radius  $6\lambda$ .

clusters out to the boundary of the barotropic vortex has occurred. The heton experiments clearly demonstrate that even when the barotropic component of the flow is not large enough to prevent instability, the lateral buoyancy fluxes are sufficiently suppressed as to have a significant influence on the density anomaly of the overturned fluid.

The heton model, due to its inherently discrete formulation, produces some spurious interactions between the vortices and the sharp front of the piece-wise constant vortex.

These tend to encourage the ejection of the anticyclonic lower-layer vortices and reduce further the baroclinicity of the convecting region. In the real ocean it is likely that the fronts of potential vorticity are not so well defined as in this piece-wise constant case; the baroclinic potential vorticity anomaly will be more evenly distributed throughout the forcing region in nature. However, despite this shortcoming, these experiments provide motivation for the further investigation of the influence of the ambient flow on the subsequent development of the dense fluid chimney in a more complete numerical formulation. They clearly suggest that the effect of the ambient flow cannot be ignored in investigations of the spreading phases of deep convection.

Under continued forcing, the baroclinic potential vorticity anomaly is continuously increasing. Obviously if the barotropic preconditioned anomaly is very small, it will have very little influence on the development of the instability, because the baroclinic anomaly will very rapidly be greater in magnitude than the pre-existing barotropic anomaly. We can estimate the magnitude of the barotropic potential vorticity anomaly necessary to influence the instability by considering the equilibrium potential vorticity anomaly achieved in the experiments of LJV when the lateral flux due to baroclinic instability completely balances the surface forcing. Then the potential vorticity anomaly of the convective region  $q^{bc} = 1.0(R_q r / \lambda)^{1/2} f = 1.2f(B_0 r / (H^3 N^3))^{1/2}$  (where the numerical constants were empirically determined). If the barotropic anomaly is greater than this value, equilibrium will not be achieved. In other words a barotropic rim current of  $U > 0.6 \times (B_0 r / (H^3 N^3))^{1/2} r f$  will be necessary to prevent instability. In the ocean, we expect  $B_0$  to be of the order of  $5 \times 10^{-8}$  to  $5 \times 10^{-7} \text{ m}^2 \text{ s}^{-3}$ ,  $N \sim 5\text{--}50 \times 10^{-4} \text{ s}^{-1}$  and  $r \sim 10^4\text{--}10^5 \text{ m}$ . Hence barotropic currents between 1–100 cm/s will be necessary to prevent instability, depending on the magnitude of the forcing and size of the vortex. Smaller radius cooling regions will have their instability suppressed by smaller magnitude barotropic currents. The corresponding barotropic vorticity anomaly may be as low as  $0.003f$ , for small radius, low forcing, and strong ambient stratification (at the limits of these parameters given above). Clearly the important nondimensional parameter describing the influence of the ambient flow is

$$\frac{q^{bt}}{q^{bc}(eq)} = \frac{q^{bt}}{1.2f} \left( \frac{N^3 H^3}{B_0 r} \right)^{1/2} \quad (6)$$

the ratio of the barotropic potential vorticity to the equilibrium baroclinic potential vorticity which would be obtained in the absence of ambient flow. For our examples this ratio is 1.6. Future work will investigate the dependence of flow properties on this ratio.

## 5. Conclusion

Recent numerical and laboratory studies of localized open ocean convection have identified baroclinic instability as providing a lateral flux of buoyancy, which in some cases completely offsets the surface buoyancy loss, and so limits the depth of the mixed layer and density anomaly of the overturned fluid. Here we have identified and assessed the

importance of a process which is likely to influence the efficiency of the lateral fluxes, by preventing the onset, and suppressing the development of the baroclinic instability: the barotropic vortical component of the ambient circulation. Such a barotropic circulation may exist as a component of the preconditioning necessary to localize deep convection. The preconditioned flow appears to be self-perpetuating: the net result of convection is a reinforced cyclonic vortex, because the anticyclonic component in the lower layer of the convectively generated flow is preferentially removed by the baroclinic instability. Analogously, if the preconditioned circulation is comprised predominantly of an anticyclonic component, we would expect the upper-layer fluxes to be most significant, removing the cyclonic component of the convectively generated circulation, and hence reinforcing the anticyclonic preconditioned circulation. If the preconditioned flow has a significantly larger dimension than that of the convectively generated circulation, then that flow may trap the fluid within its confines, and force its continued exposure to the surface forcing in the region.

In the ocean the interaction between baroclinic instability and barotropic circulation may be considerably more complex than studied here. The eddies generated through baroclinic instability may interact so as to generate larger-scale barotropic circulation, through merger and alignment, and this circulation may then influence instability generated by subsequent convective activity. In this sense, an oceanic analogue to the atmospheric “barotropic governor” may exist, with barotropic circulation generated through baroclinic instability ultimately influencing the efficiency of that instability.

To conclude, the presence of the preconditioned flow has a significant influence on the resulting water masses and large-scale flow, and an accurate parameterization scheme for the effects of open-ocean deep convection on the large-scale ocean circulation must account for these features correctly.

*Acknowledgments.* SL is presently supported by a NOAA climate and global change post-doctoral fellowship, administered through the Universities Corporation for Atmospheric Research. Much of this work was carried out while SL was the recipient of a NERC studentship, while a student at Imperial College, and an exchange visitor at MIT. JM was supported by the NSF. We would like to thank Glenn Flierl for his help in the understanding of the linear stability problem and Wim Verkleij for providing the original version of the contour dynamics code. Peter Rhines pointed out the similarity to the barotropic governor in atmospheric baroclinic lifecycles, and together with an anonymous reviewer made useful suggestions for improvements to the text.

## APPENDIX A

### **Linear stability analysis of a circular two-layer vortex**

We summarize the results of stability analyses of a baroclinic piece-wise constant vortex embedded within a concentric vortex containing a strong barotropic component. We briefly show how the stability analysis of Flierl (1988) can be applied to all the cases relevant to this work, and make an extension of his analysis to include a barotropic vortex which is

larger than the baroclinic vortex. The investigation of stability is confined to the scenario shown in Figure 6: a baroclinic vortex  $\mathcal{A}$  of radius  $a$ , representing the potential vorticity anomaly generated through convective overturning, is contained within a vortex  $\mathcal{B}$  of radius  $b$  which represents any preconditioned circulation. Vortex  $\mathcal{A}$  has potential vorticity  $q_a = q^{bc}$  in the upper layer, and  $q_a = -q^{bc}$  in the lower layer. Vortex  $\mathcal{B}$  has potential vorticity  $q_b$  of which two scenarios will be considered: (i)  $q_b$  is independent of  $z$  ( $q_b = q^{bt}$ ); (ii)  $q_b$  is positive in the upper layer, and zero in the lower layer ( $q_b = q^0, 0$  respectively).

Using the formulation of Flierl (1988), the matrix equation for perturbations of the vortex boundary of azimuthal mode number  $m$  can be obtained:

$$(\mathbf{V} - \Omega \mathbf{I} - \mathbf{M}^m \mathbf{Q}) \mathbf{v}_0 = 0 \quad (7)$$

where  $\mathbf{M}^m$  is the Greens function matrix appropriate for the mode number  $m$ , and  $\mathbf{I}$  is the identity matrix,  $\mathbf{V}$  is the matrix of basic state boundary velocities,  $\mathbf{Q}$  is the matrix of basic state vortex potential vorticities,  $\mathbf{v}_0$  is the vector of boundary perturbation amplitudes, and  $\Omega$  is the frequency of these perturbations (See Flierl (1988) for the detailed derivation). The vortex will be unstable to the perturbation if the disturbance grows exponentially; i.e.  $\Omega$  is imaginary and  $\Omega/i > 0$ . For nontrivial eigenvectors we obtain the eigenvalue equation

$$\text{determinant}(\mathbf{V} - \Omega \mathbf{I} - \mathbf{M}^m \mathbf{Q}) = 0. \quad (8)$$

For our two-layer, two-vortex configuration, the matrices take the following form

$$\mathbf{v}_0 = \begin{pmatrix} v_a^{bt} \\ v_b^{bt} \\ v_a^{bc} \\ v_b^{bc} \end{pmatrix} \quad (9)$$

$$\mathbf{V} = \begin{pmatrix} V_{bt}(a)/a & 0 & V_{bc}(a)/a & 0 \\ 0 & V_{bt}(b)/b & 0 & V_{bc}(b)/b \\ V_{bc}(a)/a & 0 & V_{bt}(a)/a & 0 \\ 0 & V_{bc}(b)/b & 0 & V_{bt}(b)/b \end{pmatrix} \quad (10)$$

$$\mathbf{Q} = \begin{pmatrix} q_a^{bt} & 0 & q_a^{bc} & 0 \\ 0 & q_b^{bt} & 0 & q_b^{bc} \\ q_a^{bc} & 0 & q_a^{bt} & 0 \\ 0 & q_b^{bc} & 0 & q_b^{bt} \end{pmatrix} \quad (11)$$

$$\mathbf{M}^m = \begin{pmatrix} \frac{1}{2m} & \frac{1}{2m \left(\frac{b}{a}\right)^{m-1}} & 0 & 0 \\ \frac{1}{2m \left(\frac{b}{a}\right)^{m+1}} & \frac{1}{2m} & 0 & 0 \\ 0 & 0 & I_m \left(\frac{a}{\lambda}\right) K_m \left(\frac{a}{\lambda}\right) & \left(\frac{b}{a}\right) I_m \left(\frac{a}{\lambda}\right) K_m \left(\frac{b}{\lambda}\right) \\ 0 & 0 & \left(\frac{a}{b}\right) I_m \left(\frac{a}{\lambda}\right) K_m \left(\frac{b}{\lambda}\right) & I_m \left(\frac{b}{\lambda}\right) K_m \left(\frac{b}{\lambda}\right) \end{pmatrix} \quad (12)$$

where  $I_m(x)$  and  $K_m(x)$  are the  $m$ th order modified Bessels functions, and  $\lambda$  is the effective deformation radius,  $\lambda = NH/(\sqrt{2f})$ . The subscripts *bt* and *bc* refer to the barotropic and baroclinic components respectively. Furthermore, the velocities can be expressed, in terms of the potential vorticity anomalies thus:

$$\frac{V_{bt}(a)}{a} = \frac{q_a^{bt}}{2} + \frac{q_b^{bt}}{2} \quad (13)$$

$$\frac{V_{bt}(b)}{b} = \left(\frac{a}{b}\right)^2 \frac{q_a^{bt}}{2} + \frac{q_b^{bt}}{2} \quad (14)$$

$$\frac{V_{bc}(a)}{a} = q_a^{bc} I_1 \left(\frac{a}{\lambda}\right) K_1 \left(\frac{a}{\lambda}\right) + \left(\frac{b}{a}\right) q_b^{bc} I_1 \left(\frac{a}{\lambda}\right) K_1 \left(\frac{b}{\lambda}\right) \quad (15)$$

$$\frac{V_{bc}(b)}{b} = q_a^{bc} \left(\frac{a}{b}\right) I_1 \left(\frac{a}{\lambda}\right) K_1 \left(\frac{b}{\lambda}\right) + q_b^{bc} I_1 \left(\frac{b}{\lambda}\right) K_1 \left(\frac{b}{\lambda}\right). \quad (16)$$

We therefore have an eigenvalue problem dependent on the following variables:  $a, b, \lambda, m, q_a^{bt}, q_a^{bc}, q_b^{bt}, q_b^{bc}$ . However, we will limit our parameter space by investigating cases where  $q_a^{bt} = 0$ , and either  $q_b^{bc} = 0$  or  $q_b^{bc} = q_b^{bt}$ . For simplicity we can now define  $q^{bc} = q_a^{bc}$ , and either  $q^{bt} = q_b^{bt}$ , (case i) or  $q^{bt} = q_b^{bc} = q^0/2$  (case ii). Then the eigenvalue problem will depend on four independent variables  $b/a, a/\lambda, m$  and  $q^{bt}/q^{bc}$  or  $q^0/q^{bc}$ .

If  $a = b$ , and  $q^{bt} = 0$  we obtain the sufficient condition for instability deduced by Pedlosky (1985) and Saunders (1972):

$$I_1 \left(\frac{a}{\lambda}\right) K_1 \left(\frac{a}{\lambda}\right) < \frac{1}{2m} \quad (17)$$

For  $m \geq 2$  this approximates to

$$m < \frac{a}{\lambda}. \tag{18}$$

However the vortex is not unstable to mode number 1, since then  $\Omega \equiv 0$ . Hence a baroclinic vortex is unstable to perturbations of mode numbers  $m \geq 2$  given by (18), if  $a/\lambda > 2$ .

The growth rate of the instability, when the above condition is satisfied is

$$\Omega = q^{bc} \sqrt{\left[ (I_1 K_1 - \frac{1}{2m})(I_1 K_1 - I_m K_m) \right]} \tag{19}$$

where all Bessels functions have as their argument  $a/\lambda$ .

When  $a = b$  and  $q^{bt} \neq 0$  the sufficient condition for instability becomes:

$$\frac{q^{bt}}{q^{bc}} < \frac{\sqrt{\left[ 4(I_1 K_1 - I_m K_m) \left( \frac{1}{2m} - I_1 K_1 \right) \right]}}{\frac{1}{2m} - I_m K_m} \tag{20}$$

when  $q^{bt}/q^{bc} > 0$ . The limiting value of  $q^{bt}/q^{bc}$  for instability is shown plotted in Figure 16a, as a function of mode number  $m$ , for the specific case of  $a/\lambda = 5.0$  (as in our heton simulations). If the barotropic component  $q^{bt}$  is greater than this limiting value, baroclinic instability will be prevented. For the most unstable mode-number  $m$ , (20) reduces to  $q^{bt}/q^{bc} < 1$ , which is the necessary condition for instability given by the Charney-Stern theorem (Charney and Stern, 1962). For smaller values of  $q^{bt}/q^{bc}$ , the growth rate of the instability is reduced (Fig. 17):

$$\Omega = \frac{1}{2} \sqrt{\left[ 4(q^{bc})^2 \left( I_1 K_1 - \frac{1}{2m} \right) (I_1 K_1 - I_m K_m) - (q^{bt})^2 \left( \frac{1}{2m} - I_m K_m \right)^2 \right]} \tag{21}$$

In contrast, if the vortex consists of a baroclinic part  $q^{bc}$  plus an additional positive component  $q^0$  in the upper layer only, the sufficient condition for instability becomes:

$$\frac{q^0}{q^{bc}} < \frac{4(I_1 K_1 - I_m K_m) \left( \frac{1}{2m} - I_1 K_1 \right) + 2 \left( \frac{1}{2m} - I_m K_m \right) \sqrt{\left[ (I_1 K_1 - I_m K_m) \left( \frac{1}{2m} - I_1 K_1 \right) \right]}}{\frac{1}{2} \left[ \left( \frac{1}{2m} - I_m K_m \right)^2 - 4(I_1 K_1 - I_m K_m) \left( \frac{1}{2m} - I_1 K_1 \right) \right]} \tag{22}$$

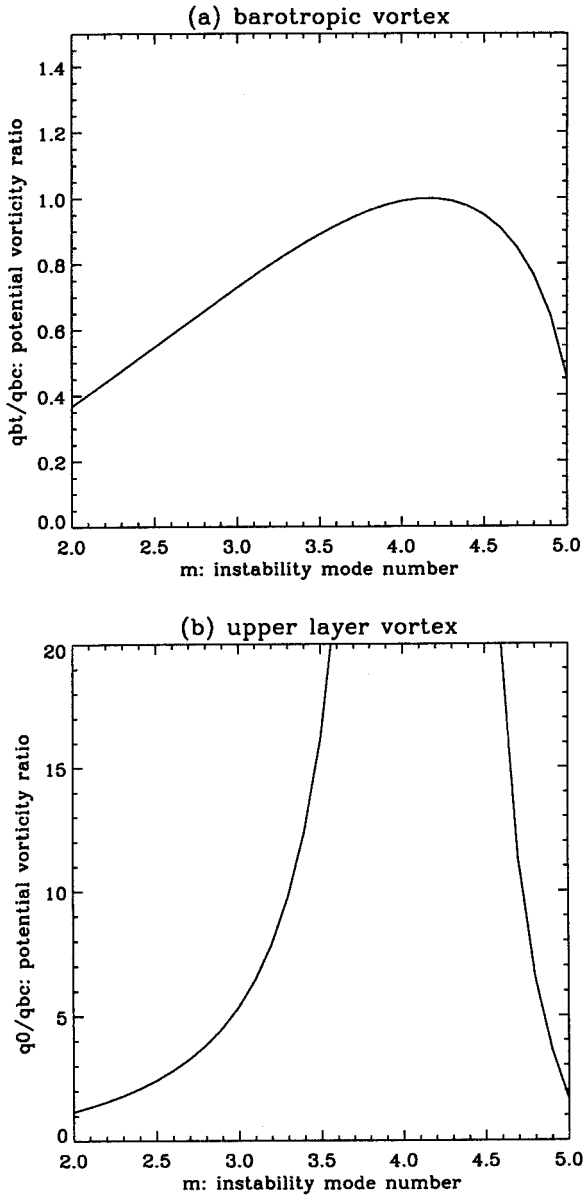


Figure 16. The limiting values of (a)  $q^{bt}/q^{bc}$  and (b)  $q_o/q^{bc}$  above which instability does not occur, as a function of mode number  $m$ , for  $a/\lambda = 5.0$ , when the radii of the additional vortex component is equal to that of the baroclinic vortex ( $b = a$ ). The fastest growing mode ( $m \approx 4$ ) is suppressed when  $q^{bt}/q^{bc} = 1.0$ , but only at infinitely high  $q_o/q^{bc}$ .

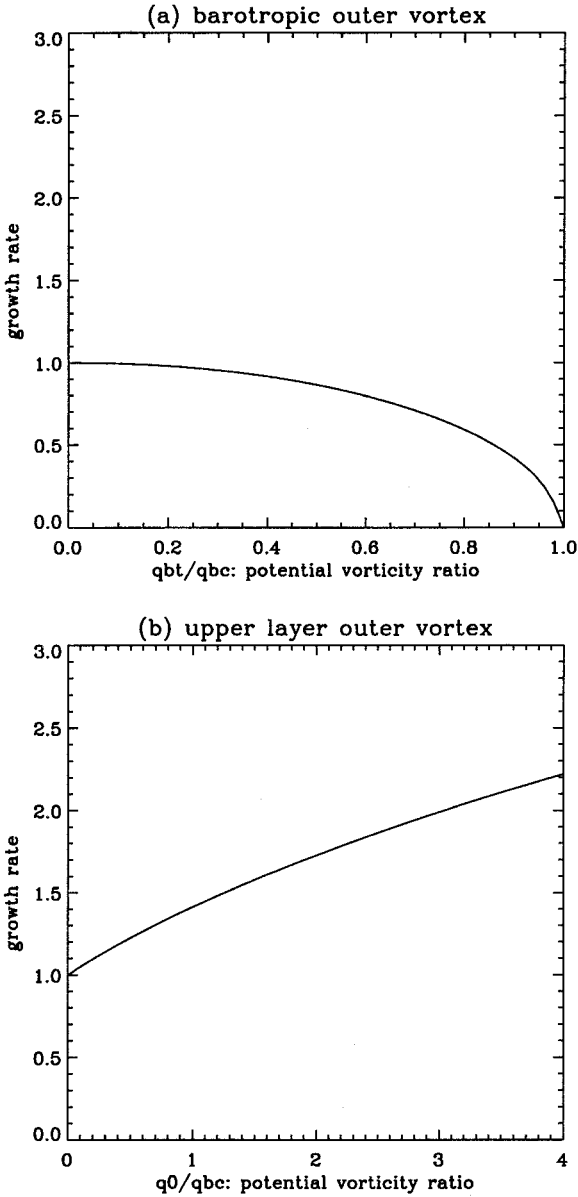


Figure 17. The growth rate, nondimensionalized by the growth rate for a purely baroclinic vortex, as a function of (a)  $q^{bt}/q^{bc}$  and (b)  $q_0/q^{bc}$ , for the fastest growing mode. The radii of the additional vortex component is equal to that of the baroclinic vortex ( $b = a$ ),  $m = 4$  and  $a/\lambda = 5$ .

with the limiting value for instability shown plotted against mode number  $m$  in Figure 16b for  $a/\lambda = 5.0$ . For the most unstable mode number, there is no limiting value of  $q^0$  at which instability is suppressed. Note that the Charney-Stern necessary condition for instability is always satisfied in this case.

Although the instability is never suppressed, the growth rate is modified:

$$\Omega = \frac{1}{2} \sqrt{4 \left( q^{bc} + \frac{q_0^2}{2} \right) \left( I_1 K_1 - \frac{1}{2m} \right) (I_1 K_1 - I_m K_m) - \frac{q_0^2}{4} \left( \frac{1}{2m} - I_m K_m \right)^2} \quad (23)$$

However, for the most unstable mode number, this corresponds to an increase in growth rate, rather than a decrease.

Finally, we examine the case where  $a \neq b$ . If, as in case (i),  $q_a^{bt} = 0$  and  $q_b^{bc} = 0$ , the eigenvalue equation (8) becomes

$$\det \begin{pmatrix} \frac{q}{2} - \omega & \frac{-q}{2m\beta^{m-1}} & I_1 K_1 - \frac{1}{2m} & 0 \\ 0 & \frac{q}{2} \left( 1 - \frac{1}{m} \right) - \omega & \frac{-1}{2m\beta^{m+1}} & \frac{1}{\beta} I_1 K_1 \left( \frac{b}{\lambda} \right) \\ I_1 K_1 - I_m K_m & 0 & \frac{q}{2} - \omega & -q\beta I_m K_m \left( \frac{b}{\lambda} \right) \\ \frac{-1}{\beta} I_m K_m \left( \frac{b}{\lambda} \right) & \frac{1}{\beta} I_1 K_1 \left( \frac{b}{\lambda} \right) & 0 & q \left( \frac{1}{2} - I_m \left( \frac{b}{\lambda} \right) K_m \left( \frac{b}{\lambda} \right) \right) - \omega \end{pmatrix} = 0 \quad (24)$$

where  $q = q^{bt}/q^{bc}$ ,  $\beta = b/a$ ,  $\omega = \Omega/q^{bc}$ . All Bessels functions have  $a/\lambda$  as their argument unless otherwise stated. Numerical solution of this fourth order equation for  $\omega$  shows that, as in the case where  $b = a$ , a sufficiently large barotropic component  $q^{bt}$ , will suppress the instability, provided that  $b - a$  is not much greater than a deformation radius  $\lambda$ . Figure 18a shows the numerically obtained values of  $\omega$  as a function of  $q^{bt}/q^{bc}$  and  $b/a$  for  $a/\lambda = 5.0$  and  $m = 4$  (the fastest growing mode if  $q^{bt} = 0$ ). When the barotropic vortex is large compared to the baroclinic vortex, the inner vortex feels only what amounts to a solid body rotation, which does not reduce the baroclinic instability.

For case (ii), where  $q_b = 0$  in the lower layer, we have  $q_a^{bt} = 0$ ,  $q_b^{bt} = q_0/2$ , and  $q_b^{bc} = q_0/2$ . Substituting these values into the eigenvalue equation, we again find that suppression of the instability is possible for  $b \approx a$ , although not over as large a part of the domain as in case i, and not for the most unstable mode number. Figure 18b shows the numerically obtained  $\omega$  as a function of  $q_0/q^{bc}$  and  $b/a$  for  $m = 4$  and  $a/\lambda = 5.0$ .

We conclude that the instability of a circular baroclinic vortex in a two-layer formulation of equal layer depths may be suppressed by a barotropic component of potential vorticity greater in magnitude than the baroclinic component. This result holds if the barotropic

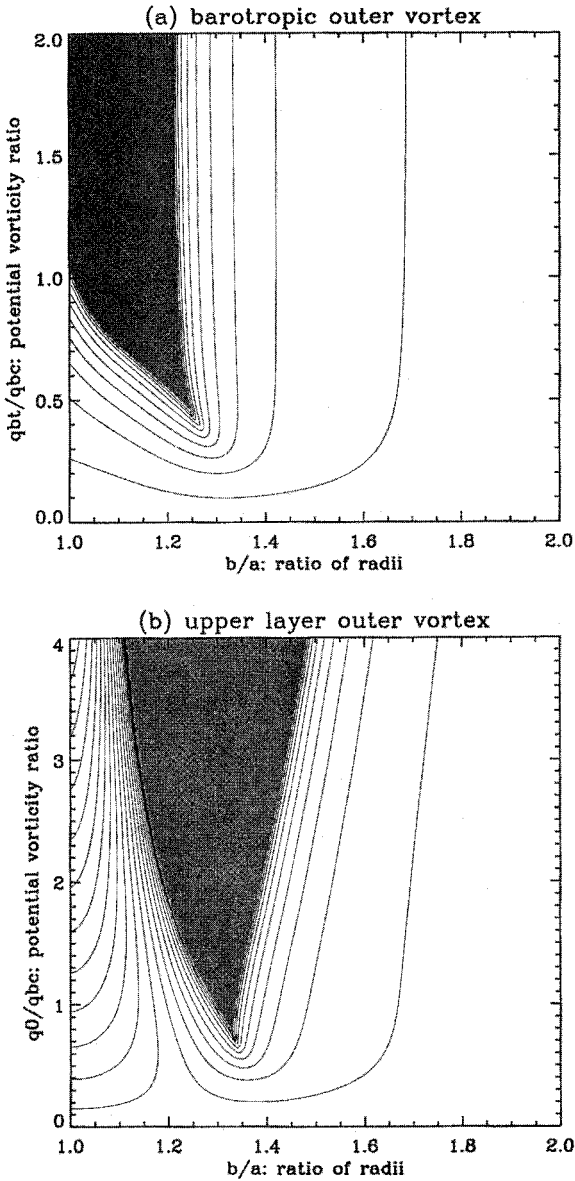


Figure 18. The growth rate of the instability  $\omega/q^{bc}$  for mode number  $m = 4$  and  $a/\lambda = 5.0$  as a function of (a)  $q^{bt}/q^{bc}$  or (b)  $q^0/q^{bc}$  and  $b/a$ . The shaded region indicates no exponential growth ( $\omega = 0$ ).

vortex is larger than the baroclinic vortex provided the radius of the larger vortex is not much more than a deformation radius greater than the radius of the inner vortex. By contrast the addition of a cyclonic component in the upper layer alone does not suppress the instability of the fastest growing mode.

## APPENDIX B

**Contour dynamics**

We use contour dynamical techniques as developed by Zabusky *et al.* (1979), to study the evolution of the piece-wise constant vortex and its interaction with the point vortices. The boundary of the vortex is represented by a finite number of discrete nodes and it is sufficient to determine the self-advection of these boundary nodes to study the flow evolution, thereby reducing the problem from one of three dimensions to one of two dimensions. As the integration proceeds, the boundary of the vortex becomes increasingly contorted. In order to resolve these contortions it is necessary to increase the number of nodes and to rearrange them so that they are evenly distributed, an operation which is carried out at each time-step. However, this increase in node number causes the time for the integration to run to increase geometrically as it proceeds. Hence in order to reduce the integration time to manageable proportions, a “surgery” algorithm (Dritschel, 1989) is adopted, eliminating thin filaments of vorticity and thereby significantly reducing the total length of the vortex boundary. We have employed a particularly severe form of this algorithm, so that filaments are removed immediately. Since an important motivation behind the heton model is the efficiency with which solutions may be computed on small platforms, we do not wish to combine it with a form of contour dynamics which would eliminate this advantage. This reduces the accuracy of the integration, but these experiments still provide a useful guide to possible features of the large-scale behavior of both the ocean and its representation in more complex numerical models.

## REFERENCES

- Alverson, K. and W. Owens. 1996. Topographic preconditioning of open ocean deep convection. *J. Phys. Oceanogr.*, *26*, 2196–2213.
- Bretherton, F. P. 1966. Critical layer instability in baroclinic flows. *Quart. J. R. Meteorol. Soc.*, *92*, 325–334.
- Brickman, D. 1995. Heat flux partitioning in open-ocean convection. *J. Phys. Oceanogr.*, *25*, 2609–2623.
- Charney, J. G. and M. E. Stern. 1962. On the stability of internal baroclinic jets in a rotating atmosphere. *J. Atmos. Sci.*, *19*, 159–172.
- Clarke, R. A. and J.-C. Gascard. 1983. The formation of Labrador Sea Water. Part I: Large-scale processes. *J. Phys. Oceanogr.*, *13*, 1764–1778.
- Coates, M. J., G. N. Ivey and J. R. Taylor. 1995. Unsteady, turbulent convection into a rotating, linearly stratified fluid: modeling deep ocean convection. *J. Phys. Oceanogr.*, *25*, 3032–3050.
- Dritschel, D. 1989. Contour surgery: a contour dynamics method for long-time behavior of inviscid, two-dimensional rotational flow. *J. Comput. Phys.*, *77*, 240–260.
- Flierl, G. R. 1988. On the instability of geostrophic vortices. *J. Fluid Mech.*, *197*, 349–388.
- Gordon, A. L. 1978. Deep Antarctic convection west of Maud Rise. *J. Phys. Oceanogr.*, *8*, 600–612.
- Helfrich, K. R. and U. Send. 1988. Finite-amplitude evolution of two-layer geostrophic vortices. *J. Fluid Mech.*, *197*, 331–348.
- Hogg, N. G. 1973. The preconditioning phase of MEDOC 1969: II. Topographic effects. *Deep-Sea Res.*, *20*, 449–459.

- Hogg, N. G. and H. M. Stommel. 1985. Hetonic explosions: the breakup and spread of warm pools as explained by baroclinic point vortices. *J. Atmos. Sci.*, *42*, 1465–1476.
- Ivey, G. N., J. R. Taylor and M. J. Coates. 1995. Convectively driven mixed layer growth in a rotating, stratified fluid. *Deep-Sea Res.*, *42*, 331–349.
- James, I. N. 1987. Suppression of baroclinic instability in horizontally sheared flows. *J. Atmos. Sci.*, *44*, 3710–3720.
- Jones, H. and J. Marshall. 1993. Convection with rotation in a neutral ocean; a study of open-ocean deep convection. *J. Phys. Oceanogr.*, *23*, 1009–1039.
- Killworth, P. D. 1983. Deep convection in the world ocean. *Rev. Geophys. Space Phys.*, *21*, 1–26.
- Lazier, J. R. L. 1973. The renewal of Labrador Sea Water. *Deep-Sea Res.*, *20*, 341–353.
- Legg, S., H. Jones and M. Visbeck. 1996. A heton perspective of baroclinic eddy transfer in localized ocean deep convection. *J. Phys. Oceanogr.*, *26*, 2251–2266.
- Legg, S. and J. Marshall. 1993. A heton model of the spreading phase of open-ocean deep convection. *J. Phys. Oceanogr.*, *23*, 1040–1056.
- Legg, S., J. McWilliams and J. Gao. 1998. Localization of deep ocean convection by a geostrophic eddy. *J. Phys. Oceanogr.*, (in press).
- Madeo, G., F. Lott and M. Crepon. 1996. Large-scale preconditioning of deep-water formations in the Northwestern Mediterranean sea. *J. Phys. Oceanogr.*, *26*, 1393–1408.
- Nakamura, N. 1993. An illustrative model of instabilities in meridionally and vertically sheared flows. *J. Atmos. Sci.*, *50*, 357–375.
- Pedlosky, J. 1985. The instability of continuous heton clouds. *J. Atmos. Sci.*, *42*, 1477–1486.
- Pinardi, N. and A. Navarra. 1993. Baroclinic wind adjustment processes in the Mediterranean Sea. *Deep-Sea Res.*, *40*, 1299–1326.
- Saunders, P. 1973. The instability of a baroclinic vortex. *J. Phys. Oceanogr.*, *15*, 258–272.
- Send, U. and J. Marshall. 1995. Integral effects of deep convection. *J. Phys. Oceanogr.*, *25*, 855–872.
- Seung, Y.-H. 1987. A buoyancy flux-driven cyclonic gyre in the Labrador Sea. *J. Phys. Oceanogr.*, *17*, 134–146.
- Stone, P. H. 1972. A simplified radiative-dynamical model for the static stability of rotating atmospheres. *J. Atmos. Sci.*, *29*, 405–418.
- Swallow, J. C. and G. F. Caston. 1973. The preconditioning phase of Medoc 1969. I. Observations. *Deep-Sea Res.*, *20*, 429–448.
- Visbeck, M., J. Marshall and H. Jones. 1996. Dynamics of isolated convective regions in the ocean. *J. Phys. Oceanogr.*, *26*, 1721–1734.
- Zabusky, N. J., M. H. Hughes and K. V. Roberts. 1979. Contour dynamics for the Euler equations in two dimensions. *J. Comput. Phys.*, *30*, 96–106.
- Zavatarelli, M. and G. L. Mellor. 1995. A numerical study of the Mediterranean Sea circulation. *J. Phys. Oceanogr.*, *25*, 1384–1414.